INTERNATIONAL JOURNAL FOR NUMERICAL METHODS IN FLUIDS, VOL. 6, 113–127 (1986)

A THREE-DIMENSIONAL SIMULATION OF WIND FLOW AROUND BUILDINGS

T. HANSON, D. M. SUMMERS AND C. B. WILSON

Department of Architecture, University of Edinburgh, 20 Chambers Street, Edinburgh EH1 1JZ, Scotland

SUMMARY

The steady Navier–Stokes equation is solved to simulate the wind-flow environment of three-dimensional configurations of buildings. The method assumes an incident wind described by a power-law velocity profile. A new method for controlling the two-part nested solution iteration is introduced. The simulation is compared to some published wind-tunnel measurements.

KEY WORDS Wind Engineering Control Volume Method Wind Flow Simulation

INTRODUCTION

The prediction of the exposure of buildings to wind is a significant factor in assessing their energy performance, and the conditions of comfort in the spaces surrounding buildings are dependent upon the structure of the perturbed wind flow which these buildings create. For these and other reasons the problem of air flow around configurations of large-scale bluff bodies continues to attract interest. In order to understand the environmental implications of a proposed building, it would be useful for a designer to have an estimate of its effect on the wind in interaction with its surroundings. Ideally, as a preliminary guide, a designer should have available a systematic compilation of environmental wind effects for a wide variety of building shapes and configurations.

Of course the flow of air with a prescribed velocity profile, and with an arbitrary direction of incidence, over even a single bluff body is a problem of considerable physical complexity: when this problem is extended to an arbitrary configuration of bluff bodies, this complexity is obviously compounded. Typically the problem has been studied using material scale models of buildings in wind-tunnels. The task of constructing a series of scale-model experiments to explore systematically the general 'model space' of a collection of buildings is laborious because of the multiplicity of configurations which must be investigated. Furthermore, wind-tunnel experiments require resources of time and expertise which are often not available to architects and planners working within commercial constraints.

Thus a reliable computer simulation of wind flow around groups of three-dimensional bluff bodies can make a contribution to this problem by facilitating a less time-consuming exploration of the model space. In principle, a computer wind-flow simulation can make wind-related design information accessible to an architect at every stage of the design process.

What is required in this context is a numerical solution to the Navier–Stokes equation, together with the mass continuity equation, which can accurately predict the gross features of the flow field surrounding a building group. The accuracy with which a wind-tunnel can simulate full-scale flow is estimated to be about 20 per cent,[1,2] and it would be reasonable to demand of any computational

0271–2091/86/030113–15$07.50

Received 16 July 1984
Revised 2 September 1985

simulation that it approach wind-tunnel measurements to this same level of accuracy.

The aerodynamic problem is one of high Reynolds number, typically $Re \sim 10^6$. Flow separation occurs at sharp corners with zones of recirculation in the lee of the buildings. The surface boundary layer on a building is of the order of 10^{-2} m thick, whereas the atmospheric boundary layer and other large-scale features, such as the wake region, have dimensions of order 10^2 m. The disparity in these characteristic length scales makes it impracticable to resolve them simultaneously using variable grid spacing techniques. The approach adopted here has been to use a variable grid for the medium- to large-scale features, with spacings ranging from 1 to 5 metres in the vicinity of buildings and from 10 to 20 metres in the free-stream and far-wake regions. For grid points adjacent to solid surfaces appropriate frictional source terms are included in the momentum equations. This procedure effectively smears out the effects of friction over the volume of a computational 'cell' and is therefore a crude approximation to the actual flow near the building surface. However, small-scale effects are simulated without detailed resolution of the boundary layers, and the treatment provides a representation of the boundary effects which is sufficiently accurate for the present purpose.

Consistent with this treatment, which attempts to satisfy the governing physical laws macroscopically, a control volume scheme was chosen for discretization of the continuum equations. The solution method is based on that proposed by Caretto *et al.*,[3,4], for problems involving high Reynolds number, including environmental problems.[3]

In the case of a configuration of several buildings, local features can develop in the flow which can be directly related to the relative dimensions of the buildings, their geometrical shapes, and their site configuration. A particular example of such a feature is the 'reverse vortex flow' which develops in the space between two parallel buildings which are orientated perpendicular to the incident wind stream. This feature has been examined in detail by Penwarden and Wise[5] using wind-tunnel models. The parametric curves determined from these experiments (see Figure 48 in Reference 5) provide a specific indication of the relationship between the maximum reverse-flow wind speed at ground-level between the buildings and the relative heights of the buildings, their width-to-height aspect ratio, and their separation. These curves provide a direct quantitative test for the accuracy of a simulation of the flow environment of buildings.

The wind-flow field around the same two-building configuration has also been studied by sand erosion techniques.[6] The contour depiction of the flow field determined in this way can provide a further test with which to assess the usefulness of a numerical simulation.

SOLUTION METHOD

Finite difference equations

A control volume solution method has already been applied to two-dimensional architectural problems by the authors.[7] Here the method is briefly described in the context of three-dimensional problems.

An incompressible fluid occupies a three-dimensional Cartesian space (x, y, z) over a ground plane at $z = 0$ (the 'site'). One or more bluff obstacles (i.e. buildings) are located on this plane; x is considered to be the direction of the incident free-stream. The fluid, of density ρ and viscosity μ, is in time-steady motion over the buildings with velocity $\mathbf{u} = (u, v, w)$ and pressure p.

The steady Navier–Stokes equation expresses momentum conservation for the flow, e.g. in the x direction,

$$\rho\left(u\frac{\partial u}{\partial x}+v\frac{\partial u}{\partial y}+w\frac{\partial u}{\partial z}\right)-\mu\left(\frac{\partial^2 u}{\partial x^2}+\frac{\partial^2 u}{\partial y^2}+\frac{\partial^2 u}{\partial z^2}\right)+\frac{\partial p}{\partial x}=0. \tag{1}$$

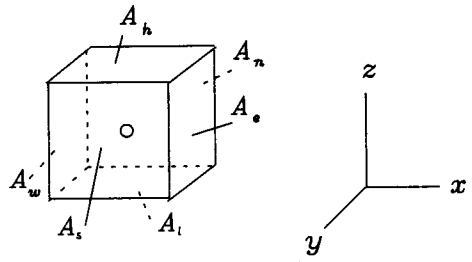

Figure 1(a). Grid nomenclature for the face areas of a control volume cell

Similar equations apply to the v and w components.

The velocity field must also satisfy conservation of mass

$$\frac{\partial u}{\partial x}+\frac{\partial v}{\partial y}+\frac{\partial w}{\partial z}=0. \tag{2}$$

To represent (1) and (2) in discrete form suitable for numerical solution we consider the solution domain to be occupied by a three-dimensional grid which defines a set of N control volumes or cells: the ith cell has dimensions $(\delta x_i, \delta y_i, \delta z_i)$. The transport of momentum by convection and diffusion between the ith cell and its six neighbouring cells is considered. Following Figure 1(a), these adjacent cells are denoted $j=$ e, w, n, s, h, l (east, west, north, south, high, low), with the area of the cell face between the ith and jth cells denoted A_j. The distance between the central node of the ith cell and that of its jth neighbour is denoted d_j.

The balance equation for u_i (the x-component of momentum per unit mass for the ith cell) consists of the following terms: (1) the rate of convective inflow of u from neighbours into i; (2) the rate of convective outflow of u from i to its neighbours; (3) the rate of diffusive transport of u into i from its neighbours; (4) internal source of u. The sum of these terms must vanish, and this balance can be denoted symbolically as

$$\sum_j c_j^{\text{in}} u_j - u_i \sum_j c_j^{\text{out}} + \sum_j D_j(u_j - u_i) + S_u = 0, \quad j = \text{e, w, n, s, h, l}, \tag{3}$$

where

$$\begin{aligned} c_j^{\text{in}} &= \rho A_j \max(0, q_j), \\ c_j^{\text{out}} &= \rho A_j \max(0, -q_j), \end{aligned} \tag{4}$$

and $q_j = -u_i, u_w, -v_i, v_s, -w_i, w_e$, for $j=$ e, w, n, s, h, l, the signs being chosen such that $q_j > 0$ implies mass inflow (see Figure 1(b)). Note that $c_j^{\text{in}} \geqslant 0$, for all j, i.e. we employ an 'upwind' formulation of the convective term.

If the velocity field is constrained to satisfy the continuity equation (2) then the outflow term may be replaced as

$$\sum_j c_j^{\text{out}} = \sum_j c_j^{\text{in}}. \tag{5}$$

The diffusive term assumes a linear relationship (Fick's law), with coefficient

$$D_j = \mu A_j / d_j. \tag{6}$$

The form of the source term S_u varies from cell to cell, depending on proximity to solid

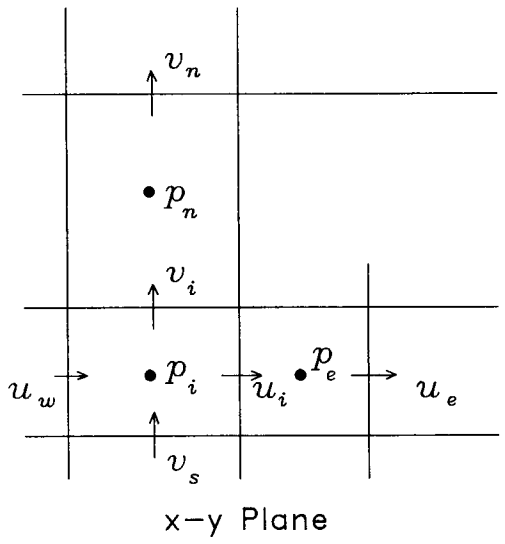

Figure 1(b). Staggered non-uniform grid in $x - y$ plane

boundaries. In general, S_u associated with the ith cell contains a pressure term

$$S_u^{\mathrm{p}} = (p_i - p_e)A_e. \tag{7}$$

In addition, for cells adjacent to solid boundaries, when considering momentum components parallel to the solid surface, a non-linear frictional shear stress term is also included

$$S_u = S_u^{\mathrm{p}} + u_i S_u^{\tau}, \tag{8}$$

where S_u^{τ} is derived from Blasius' expression for turbulent shear flow.

Using the above relations and defining local transport coefficients,

$$a_j = c_j^{\mathrm{in}} + D_j,$$

equation (3) may be rearranged to give

$$u_i^* = \frac{\sum_i a_j u_j + S_u^{\mathrm{p}}}{\sum_j a_j + S_u^{\tau}}, \tag{9}$$

where u_i^* denotes an intermediate estimate for u_i. Equations analogous to (9) may also be written for v_i^* and w_i^*.

The solution algorithm consists essentially of a 'combined iteration' scheme in which equation (9) is solved for $\mathbf{u}^* = (u^*, v^*, w^*)$ using an initial velocity field $\mathbf{u}$ which satisfies continuity. $\mathbf{u}^*$ then satisfies (9) identically but does not in general satisfy continuity, so that the net rate of mass inflow to the ith cell may be non-zero, i.e.

$$\sum_j c_j^* = \varepsilon_i^*, \tag{10}$$

where $c_j^* = \rho A_j q_j^*$, with q_j^* corresponding to the q_j defined in (4), is the convective mass inflow from the jth to the ith cell (without 'upwinding') and ε_i represents the rate of mass accumulation within the ith cell.

To eliminate ε_i^* we compute a set of pressure increments $\mathrm{d}p_i$ which, when applied to the $\mathbf{u}^*$ field, restores mass continuity, i.e.

$$q_j = q_j^* + \frac{\partial q_j^*}{\partial p}(\mathrm{d}p_i - \mathrm{d}p_j), \quad j = \mathrm{e, n, h}, \tag{11}$$

such that

$$\sum_j c_j = \sum_j \rho A_j q_j = \varepsilon_i, \tag{12}$$

where, for the present analysis, we assume $\varepsilon_i = 0$.

The partial derivative in (11) is estimated from (9) and (7), for example, as

$$\frac{\partial u^*}{\partial p} = A_\mathrm{e} \Big/ \left(\sum_j a_j + S_u^\mathrm{r} \right). \tag{13}$$

Rewriting (10) in terms of convective flows and summing over j we obtain

$$\sum_j c_j = \sum_j \left\{ c_j^* + \frac{\partial c_j^*}{\partial p}(\mathrm{d}p_i - \mathrm{d}p_j) \right\}, \tag{14}$$

where

$$\frac{\partial c_j^*}{\partial p} = \rho A_j \frac{\partial q_j^*}{\partial p}.$$

Substituting in (14) from (10) and (11) and rearranging, we obtain an expression for the pressure increment:

$$\mathrm{d}p_i = \left\{ \sum_j \frac{\partial c_j^*}{\partial p} \mathrm{d}p_j - \varepsilon_i^* \right\} \Big/ \sum_j \frac{\partial c_j^*}{\partial p}. \tag{15}$$

This is equivalent in form to the discrete approximation to a Poisson's equation, with second-order differences, and may be solved using any standard iterative method. The methods used for the inner and outer iterative procedures, and for overall control of the solution algorithm, are described later.

Following adjustment of the velocities using (11), the pressure field is updated to give a pressure distribution which, when applied during the next application of (9), will tend to reduce the ε_i^*, thus

$$p_i = p_i^* + \mathrm{d}p_i, \tag{16}$$

where p_i^* denotes the pressure field from the preceding iteration.

The use of upwind differencing of the convective terms in the momentum f.d.e.s is a source of numerical error. The formal accuracy requirement when using this method is $Re_i \ll 2$, where Re_i represents the cell Reynolds number for the ith cell and is given by $Re_i \approx u_i \delta x_i / 2$ for the x direction.

For slightly viscous flows this constraint is usually very difficult to satisfy. In such problems however the effects of large Re_i on the overall accuracy of the solution need not be critical, since the convective terms are typically two or three orders of magnitude greater than the diffusive terms. In the present work, this inequality applies everywhere in the solution domain with the exception of near-wall regions. To improve the accuracy of the solution we have replaced the physical viscosity with an effective value $\mu_\mathrm{eff} \sim 10^3\, \mu$. Although this expedient does not reduce Re_i sufficiently to meet the formal requirement, it provides plausible solutions for bluff body flows of the kind considered here.

Boundary conditions for architectural application

At the inlet (the plane $x = 0$) and outflow ($x = X$) boundaries, a velocity profile is specified which simulates the steady characteristics of an atmospheric boundary layer with power-law distribution: thus at $x = 0$ or X we have

$$\begin{aligned} u &= u_{\text{ref}}(z/z_{\text{ref}})^{\alpha}, \\ v &= 0, \\ w &= 0, \end{aligned} \tag{17}$$

where u_{ref} is the inlet stream velocity evaluated at the reference height z_{ref} and α is a prescribed exponential factor (typically $\alpha = 0{\cdot}16$ for rural wind conditions or $\alpha = 0{\cdot}28$ for suburban conditions). Precaution must be taken to place the outflow boundary well downstream of the obstacles if the wake is not be distorted by the imposition of condition (17). On the lateral extremities of the site, i.e. $y = 0$ or Y, and on its upper extremity, i.e. $z = Z$, the flow is also specified by (17): the boundary-layer flow at these perimeters of the site is considered to be unperturbed.

At the solid surfaces (i.e. $z = 0$ and on the surface of the buildings themselves) no attempt is made to represent the microscopic structure of the no-slip boundary layers which are formed there. Rather, we approximate the impermeability and no-slip conditions in the following ways. The shear stress at a solid surface is represented by Blasius' formula for a flat plate at zero incidence in turbulent flow, i.e.

$$\tau = c_{\tau} u_{\parallel}^2 / \mathrm{d}A, \tag{18}$$

where $u_{\parallel}$ denotes the velocity parallel to the surface on the outer edge of its boundary layer and c_{τ} is a constant characterizing the flow, namely

$$c_{\tau} = 0{\cdot}03(Re)^{-1/5}\rho. \tag{19}$$

In the present work the value of Re used in (19) is computed as

$$Re = \rho u_{\text{in}} L/\mu, \tag{20}$$

in which u_{in} is the average inlet free-stream velocity and L is a typical building dimension. It should be noted that the choice of parameters for calculating Re is not critical, since c_{τ} is relatively insensitive to Re. Over the range of values encountered in architectural flows, say $Re = 10^5$–10^7, c_{τ} varies only by a factor of 2·5. The momentum source associated with flow over a solid surface can now be expressed as

$$S_u^{\tau} = \int (\tau/u_{\parallel})\mathrm{d}A, \tag{21}$$

where A is the surface area of the wall. When a control volume cell is intersected by a solid boundary, the 'occluded' area, B_j of each of the cell faces is determined from the grid geometry. This can then be used to construct a discrete expression for (16), namely

$$S_u^{\tau} = c_{\tau}|u_i|\sum B_j, \tag{22}$$

where j denotes summation over all faces in planes parallel to u_i.

The impermeability condition is represented by evaluating the reduced area of each partially occluded cell, i.e. evaluating $A'_j = A_j - B_j$, and hence using these reduced areas at solid boundaries instead of A_j in equations (4)–(15).

There is no attempt to impose a conventional 'no-slip' boundary condition, i.e. $u_{\parallel} = 0$. To impose a zero slip would require fine-gridding close to the surface to achieve a reasonable approximation

to the boundary layer profile; the escalation in computation time and storage requirements would be unacceptable. The complexity of choosing a suitable gridding arrangement for buildings which were not aligned with the site axes would also increase substantially.

If the boundary conditions are such that a flow is known *a priori* to be symmetric across a plane, $y = y_s$ say, then the flow need only be solved in one half of the flow domain, i.e. in $0 < y < y_s$, or alternatively in $y_s < y < Y$. The boundary condition at $y = y_s$ is simulated by forcing the transport coefficients which control diffusive and convective transfer across this boundary to vanish.

Since the velocity field at the site boundaries always satisfies continuity, the external boundary condition for the pressure adjustment equation (15) is simply $dp = 0$. This condition must also apply for cells within solid obstacles, and is ensured by the fact that the coefficients of dp_j in (15) are set to zero for blocked cell faces.

The method can be applied to an arbitrary number of building shapes and configurations although, in the present examples, the algorithm is applied to block-shaped structures. Each building may be given an independent orientation and position within the site. In addition, three-dimensional simple convex forms can be treated as modules: by juxtaposing them, horizontally or vertically, more complicated building forms can be constructed.

Solution algorithm

The selection of solution methods for the finite difference equations (9) and (15) is determined largely by the properties of the equations themselves. However the definition of 'optimal' methods may also depend on external influences. In the present work it was most desirable that the methods used should accommodate a wide range of building shapes and configurations without user intervention.

The principal steps in the algorithm are:

(a) An initial guess for the velocity field $\mathbf{u}_0$ is obtained from a potential flow calculation. Since the inlet shear flow given by equation (17) is inappropriate to potential flow, it is temporarily replaced by uniform inlet and outlet profiles with total mass flow equivalent to that of the power-law profile. When the potential flow solution has converged the original boundary conditions are re-inserted; $\mathbf{u}_0$ then satisfies continuity everywhere except at the inlet and outlet planes. These local imbalances are quickly removed by the subsequent pressure-correction procedure (15). The pressure field is initially set to zero.

(b) Equation (9) is solved to obtain $\mathbf{u}_m^*$, where m is the outer iteration number, using a Jacobi procedure with 'under-relaxation', namely

$$u_m^* = (\mathscr{J}(\mathbf{u}_m) + \mathbf{u}_m)/2,$$

where $\mathscr{J}$ is the Jacobi operator corresponding to (9). The use of Jacobi, or some other 'simultaneous' method, ensures compliance with the continuity assumption (5), which is implicit in (9). Convergence of this scheme is assured since the iteration matrix is diagonally dominant by virtue of the source term S_u^τ in the denominator of (9), which is strictly non-negative. Convergence of the momentum equations is monitored at this point by computing residual errors, e.g. for the u-component

$$R_u = \max_i \{|u_i^*/u_i) - 1|\},$$

with $u_i > u_{\min}$ to exclude very small values in the denominator, and $u_{\min} = \sigma u_{\text{in}}$ where σ is a predetermined error level, typically 0·05.

(c) Variables required for solution of the pressure equation (15) are assembled, and the number

of iterations to be performed by the inner loop is estimated using the simple predictive procedure which is described in the next subsection. Equation (15) is then solved by successive over-relaxation using a 3-D chequerboard sweep pattern to improve convergence. A value for the relaxation parameter, $\omega = 1{\cdot}5$, was reasonably effective for a range of building configurations.

(d) The velocity and pressure fields are updated using equations (11) and (16), respectively. A residual error for pressure is also calculated:

$$R_p = \max_i \{|(\mathrm{d}p_i/p_i) - 1|\},$$

with

$$p_i > p_{\min}, \quad p_{\min} = \sigma\rho u_{\mathrm{in}}^2.$$

(e) If R_u, R_v, R_w and R_p are all less than σ then the solution is deemed to have converged and iteration is terminated; otherwise we return to step (b) and continue the process. The choice of convergence level σ is arbitrary. Accuracy may be 'traded-off' against computation time by adjustment of σ.

Control of the pressure solution

Since many iterations of the pressure correction equation (15) may be required during each cycle of the algorithm, the number of iterations of the inner loop per cycle is a factor which strongly influences the overall efficiency of the method. This efficiency can be improved by controlling the inner iteration, i.e. by allowing sufficient iterations to be performed to ensure an acceptable level of continuity, without 'oversolving' the correction equation.

A simple method has been introduced to achieve this control. The level of continuity required of a given outer iteration can be calculated as follows. The field **u** does not satisfy (5) exactly, but gives rise to a residual upwind inflow error in each cell, $\varepsilon_i^{\mathrm{in}}$ such that

$$\varepsilon_i^{\mathrm{in}} = \sum_j c_j^{\mathrm{out}} - \sum_j c_j^{\mathrm{in}}.$$

Hence (9) can be re-expressed as

$$u_i^* = \frac{\sum a_j u_j + S_u^{\mathrm{p}}}{\sum a_j + S_u^{\tau} + \varepsilon_i^{\mathrm{in}}}. \tag{23}$$

The convergence constraint

$$|\varepsilon_i^{\mathrm{in}}| \ll |\textstyle\sum a_j + S_u^{\tau}| \tag{24}$$

ensures that at each iteration the denominator of (23) does not fluctuate in a manner which will swamp the systematic convergence of **u*** and **u**. To impose (24) a normalized residual continuity error for the mth outer iteration is defined:

$$E_m = \max_i \left\{\frac{\varepsilon_i}{\sum a_j}\right\}, \quad \sum a_j \neq 0, \tag{25}$$

where ε_i is the continuity error, for the ith cell, of the adjusted velocity field as defined by (10). Neglecting source terms, the constraint (24) becomes $E_m \ll 1$ for all m. Prior to entering the pressure correction iteration, the analogous continuity error can be expressed for the 'unadjusted' field:

$$E_m^* = \max_i \left\{\frac{\varepsilon_i^*}{\sum a_j}\right\}. \tag{26}$$

Since (15) is linear in dp and the $\{\varepsilon_i\}$ are linear functions of dp by virtue of the convective mass flows, we may use E_m as an error norm. Following completion of the mth outer iteration during which n_m inner iterations have been performed, the spectral radius λ_m can be calculated from

$$\log|\lambda_m| = \{\log|E_m/E_m^*|\}/n_m, \tag{27}$$

where λ_m defined in this way is independent of source terms and so remains reasonably constant from one cycle to the next. Under the assumption $\lambda_{m+1} \approx \lambda_m$ we may predict the number of iterations required in the pressure correction in the $(m+1)$th cycle:

$$n_{m+1} = \left\{\log\left|\frac{E_{m+1}^t}{E_{m+1}^*}\right|\right\} \Big/ \log|\lambda_m|, \tag{28}$$

where E_{m+1}^t is a 'target' value of E_{m+1} which is related to the existing momentum residuals by, for example,

$$E^t = K(R_u^2 + R_v^2 + R_w^2)^{1/2}, \tag{29}$$

with, typically, $K = 0{\cdot}1$. As the iteration proceeds and the momentum residuals decrease in magnitude, the continuity condition is thus enforced with greater strictness. The control calculation takes place entirely outside the pressure-correction iteration.

A TWO-BUILDING PROBLEM: COMPARISON WITH EXPERIMENT

A problem which has attracted considerable attention is that associated with the 'reverse vortex flow' which can become established between two parallel buildings. A body of wind-tunnel data from a number of sources exists for this case to which the present simulation can be usefully compared.

We consider two rectangular buildings with dimensions $W \times D \times h$ and $W \times D \times H$, respectively. W is the common span-width of both buildings, D is their streamwise thickness, h is the building height of the upstream building, and H that of the building downstream. We consider the case $H > h$. The two buildings are aligned parallel to each other and the whole configuration is orientated perpendicular to the incident wind stream. The buildings have a common axis of bilateral symmetry, and are separated by a distance L in the stream direction (i.e. in the x-direction).

The control volume solution of this problem should supply us with a flow field solution, **u**, and pressure field, p, in the half-plane of symmetry. One of the considerable advantages of a numerical simulation of such a flow is that this can be inspected graphically at will. Because the fields typically include a complicated wake structure, a clear graphical visualization of the complete three-dimensional flow space is often difficult to achieve. In these cases the flow patterns can be more usefully depicted through a plane-by-plane inspection of the flow.

Figures 2–5 illustrate the solutions for the two-building configuration described, with the following building parameters: $W = 60\,\text{m}$, $D = 17\,\text{m}$, $L = 60\,\text{m}$, $H = 60\,\text{m}$, $h = 12\,\text{m}$. The inlet stream has an unperturbed profile given by (17) with $\alpha = 0{\cdot}16$, $u_{\text{ref}} = 5\,\text{m/s}$ and $z_{\text{ref}} = 10\,\text{m}$. The solution was determined on a $41 \times 20 \times 19$ site grid, which implies 15,580 grid cells in total. Convergence was achieved after 302 outer cycles of the momentum iteration, with residuals $(R_u, R_v, R_w, R_p) = (0{\cdot}046, 0{\cdot}0075, 0{\cdot}023, 0{\cdot}0005)$. This computation required 445 minutes of batch time on a DEC System 10.

The flow can be depicted by considering any plane (conveniently one parallel to one of the grid planes) and constructing a streakline illustration of the flow. This is achieved by following over a few time steps the paths of an array of massless particles which are released into the flow from the chosen plane. For example, Figure 2 illustrates the streaklines released from the plane $z = 2\,\text{m}$, i.e.

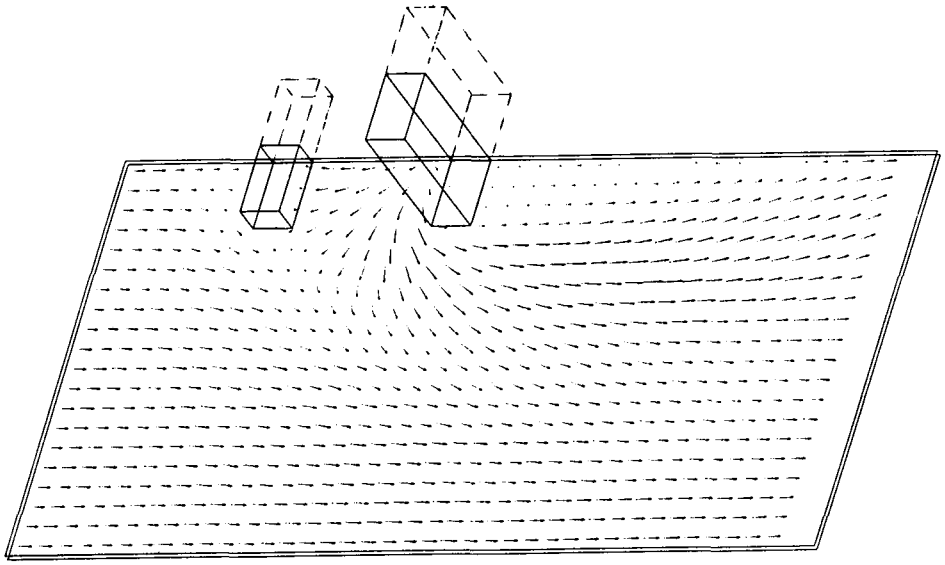

Figure 2. Streakline visualization of the simulated wind speed at ground level around a configuration of two parallel buildings

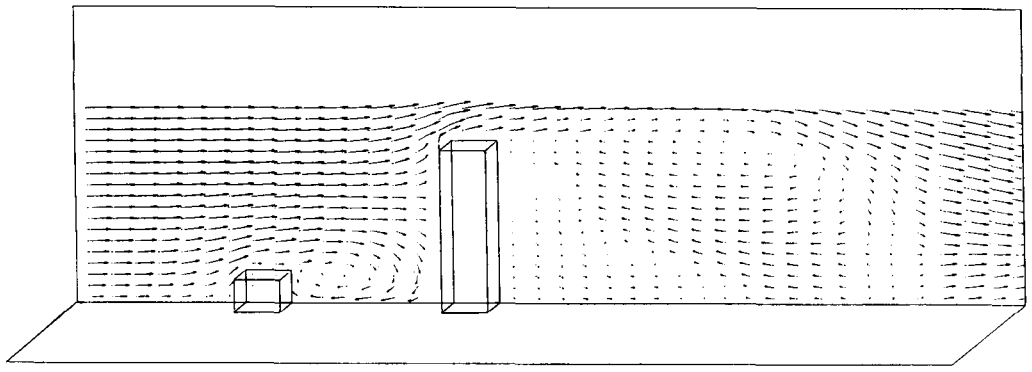

Figure 3. Elevation view of the flow: the streaklines released from a plane along the flow axis of symmetry

the plane 2 m above the ground. (We refer to the flow on this plane as the ground-level wind flow.) Both the reverse flow between the parallel buildings and the recirculation of the wake can be observed in Figure 2.

Figure 3 illustrates the streakline pattern in a streamwise elevation for a plane one metre from the plane of symmetry of the flow. This diagram shows more clearly the vertical character of the stationary reverse-vortex which is formed between the buildings, the shear separation from the lee corner of the tall building, and the general recirculation of the flow downstream of the buildings. In addition to the larger clockwise recirculation zone, there appears to be also a smaller reverse eddy immediately behind the lee face at ground level. (This latter feature can be compared with the anti-clockwise eddy which Davies *et al.*[8] observe in the near wake of a single building of height H for a 'smooth uniform' incident stream. This stream in fact has a boundary layer formed of thickness

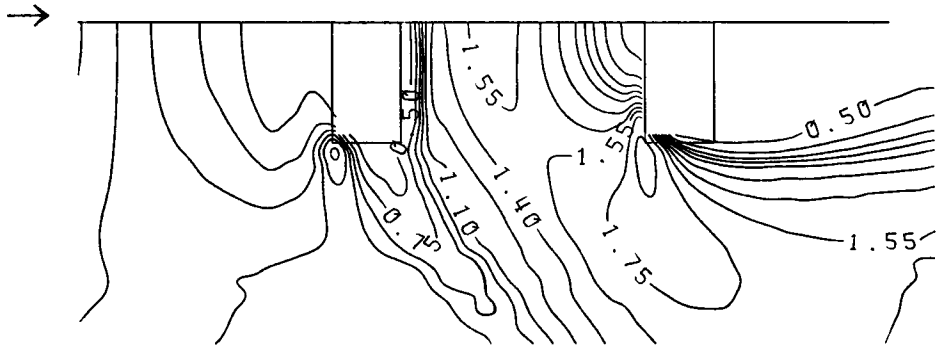

Figure 4(a). Contour map of simulated ground-level wind speeds (normalized with respect to upstream value)

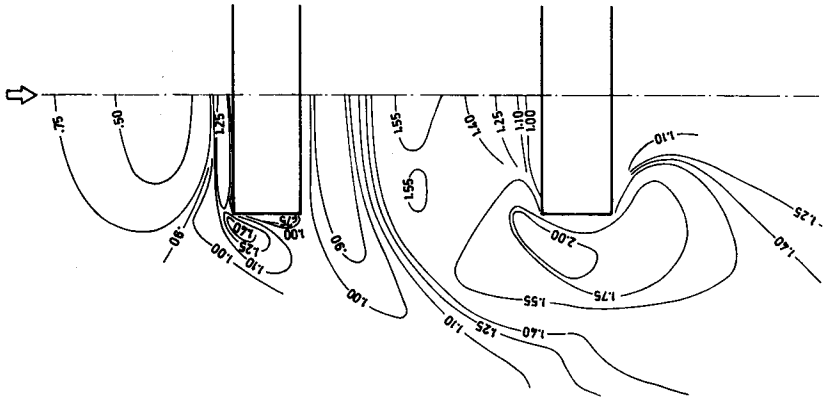

Figure 4(b). For the same building configuration, a contour map of friction velocities determined by sand saltation experiments (from Borges and Saraiva, 1980)[6]

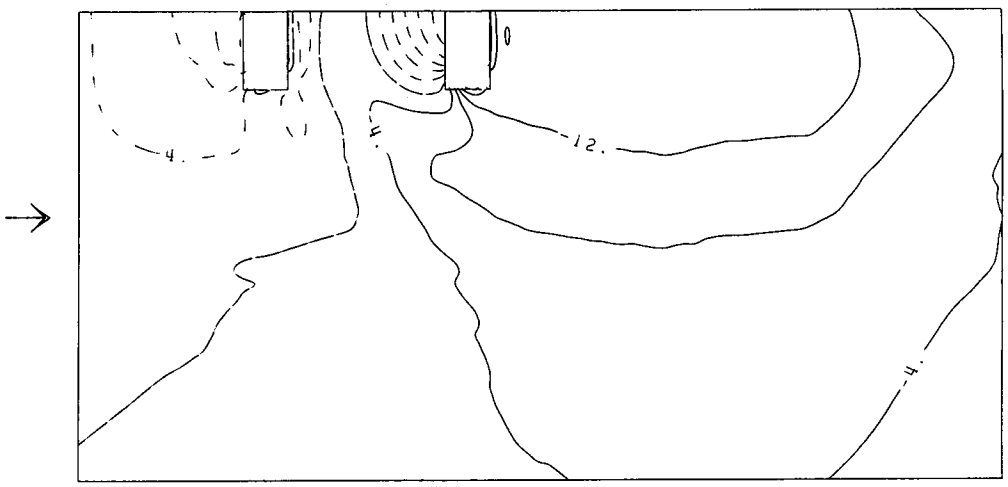

Figure 5. Contour map of pressure field (referenced to upstream value). Dashed lines represent positive pressure; solid contours represent negative pressure

$0{\cdot}2\,H$. It is interesting to speculate whether in the present case of a building upstream of height $0{\cdot}2\,H$, there are effectively re-created the shear conditions upstream which give rise to an anti-clockwise eddy in the immediate lee of the tall building.) Figure 3 can be compared to the smoke particle visualization of the problem in Figure 2 of Reference 5, or Figure 1 of Reference 9.

The flow can also be depicted graphically by constructing an interpolated contour map of the velocity and pressure fields in a given grid plane. Figure 4(a) illustrates the velocity contours 2 m from the ground plane. This map represents the contoured values of the modulus of the velocity normalized with respect to their unperturbed upstream values. The large contours at the windward corners of the buildings should be noted, as well as the stagnation at the windward face of the low building. The structure of the reverse vortex flow between the buildings may also be observed.

The contouring levels in Figure 4(a) have been chosen to allow a direct numerical comparison to be made with the wind-speed contour map published by Borges and Saraiva[6] (see their Figure 5). This map, reproduced here in Figure 4(b), is determined from the scour patterns formed by the saltation of fine grains of sand distributed over the ground plane of a wind-tunnel scale-model experiment. The scour patterns created by successively increased free-stream flow give a quantitative indication of the friction velocity on the ground plane surrounding a building configuration. For the same configuration and incident flow conditions (leaving aside the turbulence representation), it can be seen from Figure 4 that the control volume simulation we present does show encouraging numerical agreement with the experimentally-determined flow field. Such a comparison must be made with the realization that the fine-structure of both contour maps may depend upon the distribution of measurement points and the method of interpolation. Furthermore the correlation between the friction velocity determined from a scale model sand saltation experiment, and the wind speed at a height of 2 m from the ground in a full-scale case, must remain a matter of uncertainty. The agreement depicted in Figure 4 may lend encouragement to both methods for determining ground speeds around buildings. Figure 4 can also be compared to the oil film representation of this field (see Figures 3 and 4 in Reference 5). It can be noted that the shear separation from the leeward corners of the taller building is sharper in both the oil-film visualization and computer simulation that it is in the case of the sand erosion experiment. In Figures 3 and 4 the centre position of the reverse vortex lies closer to the upstream building than to the downstream one; this feature is also evident in the illustrations in Reference 5, although it is not so obvious from the sand erosion experiment in Reference 6.

A similar map of the numerically simulated pressure field at height $z = 2$ m is illustrated in Figure 5. The dashed contours represent pressure which is positive relative to an upstream reference pressure; the solid contours represent negative pressures. The pressure on the windward face of both buildings indicates a positive stagnation pressure. On the immediate leeward faces of both buildings a negative (i.e. suction) pressure develops, although in the space between the buildings this is relatively slight; a stronger suction field develops to the lee of the taller building.

A more systematic and thorough comparison of the present simulation to experimental measurement can be achieved by deriving analogous parametric curves to the wind-tunnel studies published by Penwarden and Wise[5] in their Figure 48. For these curves, the maximum reverse-flow speed at the ground level between the buildings is normalized with respect to the free-stream speed at height $z = H$ (i.e. at the height of the taller building). This ratio is then plotted as a function of width-to-height aspect ratio, W/H; this is presented in Reference 5 for four values of the separation-to-height ratio, L/H. Each measurement curve encompasses a range of values of H/h, i.e. the ratio of building heights. This range is, for the most part, $2 \leqslant H/h \leqslant 8$. The authors point out that the curves were determined for a windward building height, h, which was not much varied in the course of the parametric study. Furthermore they seem to suggest that the widths of the two buildings may have been made to differ from each other in the course of the study.

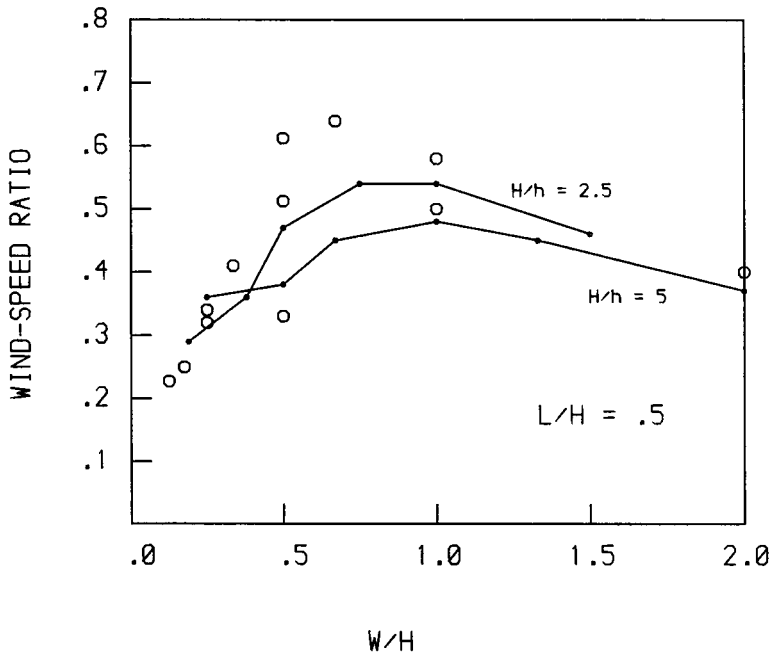

Figure 6. The case $L/H = 0{\cdot}5$. Maximum reverse vortex speed at ground level (normalized with respect to velocity at $z = H$). Comparison of wind tunnel measurement for $2 < H/h < 8$ (open circles) with two computer simulation curves for $H/h = 5$ and $H/h = 2{\cdot}5$ (solid lines)

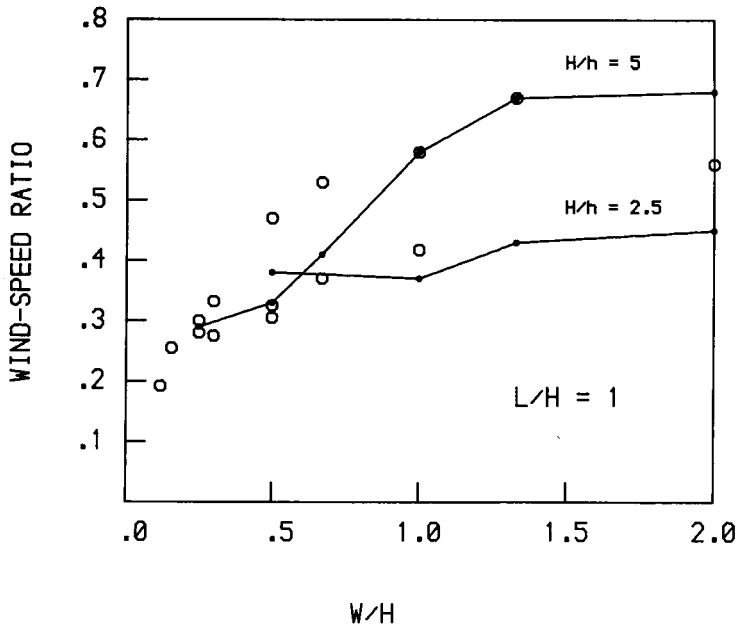

Figure 7. As Figure 6 with $L/H = 1{\cdot}0$

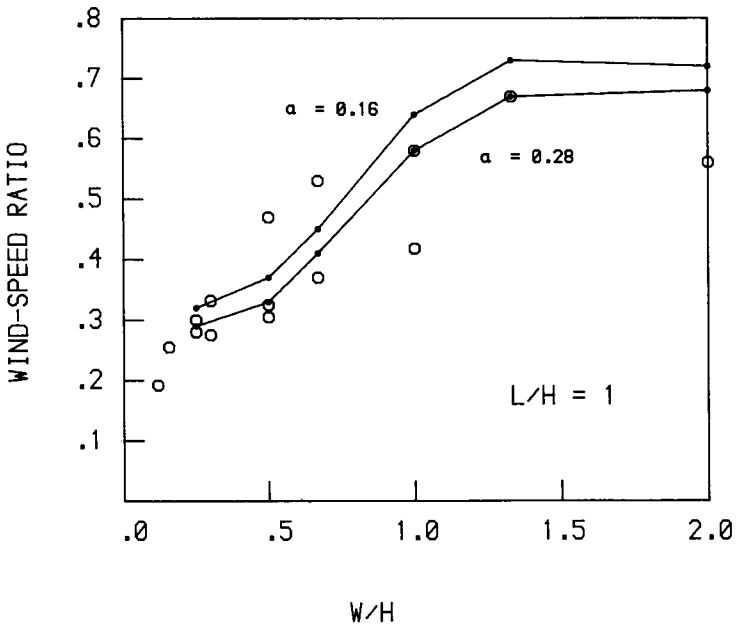

Figure 8. Comparison of two computer simulations for $L/H = 1$, $H/h = 5$, with $\alpha = 0{\cdot}16$ (upper solid curve) and $\alpha = 0{\cdot}28$ (lower curve)

We have attempted a comparison with two of the curves presented by Penwarden and Wise, namely those associated with $L/H = 1{\cdot}0$ and $L/H = 0{\cdot}5$. (The incident free stream for these particular comparisons is of power $\alpha = 0{\cdot}28$.) Figure 6 shows the comparison between wind-tunnel measurements (open circles) and our computational model (solid lines) for the case $L/H = 0{\cdot}5$. The two solid curves correspond to the two cases $H/h = 5$, and $H/h = 2{\cdot}5$. Figure 7 illustrates the same comparison for the case $L/H = 1{\cdot}0$.

It should be noted that the strength of a reverse-flow vortex depicted as a function of the ratio W/H strongly reflects the three-dimensional character of this flow. Were W/H to tend to infinity, the flow would tend to the limiting case of two-dimensionality. A two-dimensional vortex is confined to a single plane since there is no spanwise component to the flow. It can be seen from Figure 2 (where $W/H = 1{\cdot}0$) that there develops a significant component of spanwise flow as W/H becomes less than 2. In addition to the vertical vortex eddy, fluid becomes drawn laterally from the inter-building corridor. This can 'drive' the mechanism of the vortex, resulting in the broad 'maxima' evident in Figure 48 of Reference 5. On the other hand, as W/H tends to zero, the vertical component of the flow becomes dominated by spanwise motion, and the reverse-flow vortex becomes less prominent.

Penwarden and Wise have not published the specific values of H/h corresponding to the individual measurement points illustrated in Figures 6 and 7. The very close agreement in the particular case $H/h = 5$, $L/H = 1$, suggests that these model parameters do indeed correspond to the relevant data points. Even in cases where agreement is less striking, the comparison is encouraging. With few exceptions the computed values of the velocity ratio lie within a 20 per cent error band of their nearest experimental point. Both experimental and computational curves are very sensitive to error in the normalizing free-stream velocity (such error could shift the curves upwards or downwards). Furthermore, no attempt was made to reproduce numerically the specific turbulence character of the incident stream of the wind-tunnel. (Penwarden and Wise do not

indicate the specific turbulence conditions of their flow.) It remains to be seen how particular turbulence models can affect the flow environment of model buildings; the agreement achieved in the present exercise suggests that so far as the reverse-vortex flow is concerned, the turbulence in the incident stream may be a secondary influence.

Figure 8 illustrates the effect of varying the inlet profile on the parametric curve of Figure 7. We consider the case $H/h = 5$, $L/H = 1$. The upper curve is for the case $\alpha = 0{\cdot}16$ and the lower curve for $\alpha = 0{\cdot}28$. Contrasted with the effect of varying a building parameter such as H/h, the change in the incident stream appears to have less effect on the parametric curve. This is the same conclusion which Morgan and Wilson[10] reached after a wind-tunnel investigation of the same two-building configuration.

CONCLUSIONS

A control volume method has been applied to the problem of predicting the steady-state wind environment of a collection of buildings. For architectural purposes, it is required that the gross features of the flow environment be simulated to within some 20 per cent of wind-tunnel measurements. Some comparisons with wind-tunnel measurements are presented, and these indicate that simulation can reproduce the flow to within the desired accuracy. The present comparisons are of a preliminary nature; an experimental investigation is now in progress which is designed to provide a more detailed validation.

ACKNOWLEDGEMENT

This work was supported by the U.K. SERC (research grant GR/A/86329).

REFERENCES

1. P. M. Jones and C. B. Wilson, 'Wind flow in an urban area: comparison of full scale and model flows', *Build. Sci.*, **3**, 31–40 (1968).
2. R. C. F. Dye, 'Comparison of full-scale and wind-tunnel model measurements of ground winds around a tower building', *J. Wind Eng. Ind. Aerodyn.*, **6**, 311–326 (1980).
3. L. S. Caretto, A. D. Gosman, S. V. Patankar and D. B. Spalding, 'Two calculation procedures for steady three-dimensional flows with re-circulation', *Proc. 3rd Int. Conf. Num. Methods Fluid Mech.*, Springer-Verlag, Berlin 1972, pp. 60–68.
4. L. S. Caretto, R. M. Curr, and D. B. Spalding, 'Two numerical methods for three-dimensional boundary layers', *Comput. Methods Appl. Mech. Eng.*, **1**, 39–57 (1972).
5. A. D. Penwarden and A. F. E. Wise, *Wind Environment around Buildings*, HMSO, 1975.
6. A. R. J. Borges and J. A. G. Saraiva, 'An erosion technique for assessing ground level winds', in J. E. Cermak (ed.), *Wind Engineering*, Pergamon Press, 1980, p. 235.
7. T. Hanson, D. M. Summers, and C. B. Wilson, 'Numerical modelling of wind flow over buildings in two-dimensions', *Int. j. numer. methods fluids*, **4**, 25–41 (1984).
8. M. E. Davies, V. G. Quincey, and S. J. Tindall, 'The near-wake of a tall building block in uniform and turbulent flows', in J. E. Cermak (ed.), *Wind Engineering*, Pergamon Press, 1980, p. 289.
9. A. F. E. Wise, 'Effects due to groups of buildings', *Phil. Trans. Roy. Soc. Lond.*, **A269**, 469 (1971).
10. J. Morgan and C. B. Wilson, 'The effect of differently profiled wind tunnel flows on the ground level flow about model buildings', *CIRIA Report 60*, 1974.